Structural origins of intrinsic stress in amorphous silicon thin films

Eric Johlin, Nouar Tabet, Sebastián Castro-Galnares, Amir Abdallah, Mariana I. Bertoni, Tesleem Asafa, Jeffrey C. Grossman, Syed Said, and Tonio Buonassisi

Phys. Rev. B **85**, 075202 — Published 6 February 2012

DOI: 10.1103/PhysRevB.85.075202

STRUCTURAL ORIGINS OF INTRINSIC STRESS IN AMORPHOUS SILICON THIN FILMS

Eric Johlin[1*], Nouar Tabet[2], Sebastián Castro-Galnares[1], Amir Abdallah[3], Mariana I. Bertoni[1], Tesleem Asafa[2], Jeffrey C. Grossman[1], Syed Said[2], Tonio Buonassisi[1†]

[1]Massachusetts Institute of Technology, Cambridge MA 02139, USA

[2]King Fahd University of Petroleum and Minerals, Dhahran 31261, Saudi Arabia

[3]King Fahd University of Petroleum and Minerals, Center of Research Excellence in Renewable Energy, Dhahran 31261, Saudi Arabia

[*]electronic mail: johlin@mit.edu

[†]electronic mail: buonassisi@mit.edu

Abstract

Hydrogenated amorphous silicon (a-Si:H) refers to a broad class of atomic configurations, sharing a lack of long-range order, but varying significantly in material properties including optical constants, porosity, hydrogen content, and intrinsic stress. It has long been known that deposition conditions affect microstructure, but much work remains to uncover the correlation between these parameters and their influence on electrical, mechanical, and optical properties critical for high-performance a-Si:H photovoltaic devices. We synthesize and augment several previous models of deposition phenomena and ion bombardment, developing a refined model correlating plasma enhanced chemical vapor deposition (PECVD) conditions (pressure and discharge power and frequency) to the development of intrinsic stress in thin films. As predicted by the model presented herein, we observe that film compressive stress varies nearly linearly with bombarding ion momentum and with a (-1/4) power dependence on deposition pressure, that tensile stress is proportional to a reduction in film porosity, and the net film intrinsic stress results from a balance between these two forces. We observe the hydrogen bonding configuration to evolve with increasing ion momentum, shifting from a void-dominated configuration to a silicon monohydride configuration. Through this enhanced understanding of the structure-property-process relation of a-Si:H films, improved tunability of optical, mechanical, structural, and electronic properties should be achievable.

Keywords: Amorphous silicon, bandgap, curvature, density, hydrogen content, ion bombardment, PECVD, photovoltaics, porosity, pressure, stress, voids

I. Introduction

Hydrogenated amorphous silicon (a-Si:H) is an attractive photovoltaic absorber material with a large optical absorption coefficient and direct bandgap.[1,2] However, despite thirty years of research, current industrial efficiencies of large-area single-junction a-Si:H modules are barely above 6%, and the small-area laboratory record[3] stands at 9.5%, both well below the Shockley-Queisser efficiency limit of 27%.[4] Commercialization of a-Si:H has been significantly hampered by the low conversion efficiency of the material, as efficiencies above 10% are needed to offset material and manufacturing costs.[5] Knowledge of the implications of changes to deposition conditions on film properties and eventual device parameters is critical to the improvement of a-Si:H photovoltaic conversion efficiency.

There remains much to be understood concerning the structure-property-process relationships for a-Si:H thin films grown using ion deposition techniques including sputtering and plasma-enhanced chemical vapor deposition (PECVD). For instance, although the local atomic structure of amorphous silicon is known to vary widely, there are few fully accepted correlations between the atomic structure, deposition conditions, and macroscopic properties. A deeper understanding of these correlations offers a path toward a-Si:H solar cell device improvement. Herein, we synthesize an semi-empirical model describing PECVD deposited a-Si:H film stress as a function of ion bombardment and porosity, dependent on a multitude of deposition conditions, of which we focus on process pressure. We then experimentally examine the effect of ion bombardment and porosity on film intrinsic stress state. Through this analysis we are able to produce insight into the origins and influences of stress in a-Si:H films, and, by developing and correlating an empirical model describing the influence of deposition conditions on film properties and microstructure, we aim to improve the predictability of a-Si:H growth.

II. Materials and Methods

Three-inch (76 mm) diameter p-type (100) crystalline silicon substrates were used in this study. The circular geometry is advantageous when calculating stress via curvature measurements as it mitigates the intrusion of edge effects present in non-circular substrates, and the Si substrate minimizes thermal stresses due to similar coefficients of thermal expansion.

Films were deposited using a PECVD tool built by Surface Technology Systems with an RF frequency of 13.56 MHz. The baseline recipe consisted of an initial deposition of a 200 nm silicon-oxide layer to electrically isolate the film from the substrate, followed by the a-Si deposition, performed with a 200°C substrate temperature, 55 sccm pure SiH_4 flow, 200 mTorr process pressure, and 30 W power on a 182.4 cm^2 platen. From this standard recipe, several samples were deposited testing the extremes of each process condition, ensuring that for each the film (at least partially) adhered to the substrate surface. Process pressure (ranging from 100 to 1000 mTorr) was found to have

the widest range on deposited film stresses, and so was isolated as the experimental variable for this work. Resulting deposition rates (1.8–12.6 Å/s) are within range of commercial solar cell manufacturing.

Film stress can be determined by applying Stoney's formula[6] to substrate curvatures before and after thin-film deposition. Measurements of curvature were taken using a Toho FLX-2320-S, and were performed on the bare substrate, after silicon-oxide film deposition, and again after a-Si:H film deposition. Amorphous silicon film stress is then determined by comparing the change in substrate curvature before and after a-Si deposition.

The film thickness and refractive index were measured using a variable-angle spectroscopic elliposometer (M-2000XI, J.A. Woollam). To obtain the film thickness and optical constants, Kramers-Kronig relation was used to fit the measured spectra to theoretical equations for a system composed of a c-Si, silicon oxide, a-Si, silicon oxide stack.

Film density was obtained optically, using the Clausius-Mossotti relation. This describes the interaction between the index of refraction n and film density ρ,

$$\frac{n^2-1}{n^2+2}=\frac{4\pi\rho}{3M}Na \ , \qquad [1]$$

where M is the atomic mass of Si, N is Avogadro's number, and a is the atomic polarizability of the film. This latter parameter is a function of the hydrogen content (c_{H}) of the film, and has been calculated in accord with Remes[7] to be

$$\frac{n^2-1}{n^2+2}=\frac{4\pi\rho}{3M}N\left(2a_{\mathrm{Si-Si}}+\frac{c_{\mathrm{H}}}{1-c_{\mathrm{H}}}\left(a_{\mathrm{Si-H}}-\frac{a_{\mathrm{Si-Si}}}{2}\right)\right) \ , \qquad [2]$$

where the polarizability of the Si–Si and Si–H bonds in the amorphous phase are $a_{\mathrm{Si-Si}} = 1.96\times10^{-24}\,\mathrm{cm}^3$ and $a_{\mathrm{Si-H}} = 1.36\times10^{-24}\,\mathrm{cm}^3$, respectively.

Hydrogen content of the films was measured via attenuated total-reflection Fourier transformed infrared (ATR-FTIR) spectroscopy, using a PerkinElmer Spectrum 400 FT-IR spectrometer. Through the integration of the hydrogen peaks at 2000 and 2090 cm^{-1}, in the method described in Refs. 8 and 9 the total hydrogen content can be calculated, as well as the ratio of the contributions from the isolated monohydride (2000 cm^{-1}) to the polyhydride and clustered monohydride (2090 cm^{-1}), indicative of hydrogenated nanovoids, or the porosity of the films[8]. Once the hydrogen content is known, iterating the solution of **Eq. 2** allows the determination of the atomic and mass density of the film.[8,10-12] From here, the total hydrogen content, as well as the content of hydrogen bonded as Si-H (2000 cm^{-1}) and in nanovoid (2090 cm^{-1}) configurations can be obtained, the latter providing us with a quantitative measurement of film porosity. For simplicity, and due to their inherent similarity, we will use the term "hydrogen void concentration" to refer to both the atomic concentration of hydrogen in the high stretching mode configuration and the film porosity.

III. Results and Discussion

In this section we begin our analysis by investigating the physical mechanisms possible for generating stress in our a-Si thin films. We then proceed to present a model developed through the confluence of previous works and new evidence, correlating deposition conditions to two distinct forms of intrinsic stress and clarifying the origins of the observed net stress in the material.

A. Origins of Stress

Across all thin films examined here, thermal stresses ranging between +6.8 and +14.3 MPa are calculated following the method reported in Ref. 13. These stresses are small compared to total film stresses of between -1230 and +393 MPa. This result is expected due to the similar coefficients of thermal expansion[13] of silicon and amorphous silicon. Thus, we conclude that the measured stress in the films is governed by *intrinsic stress*, calculated through the subtraction of calculated thermal stress from the experimentally measured total stress. Stable films exhibit intrinsic stresses ranging from -1253 to +387 MPa (as depicted in **Fig. 1**) through the modification of process pressure. Outside this stress range, film buckling (compressive failure mode, **Fig. 2a**) and delamination (tensile failure mode, **Fig. 2b**) are observed.

Intrinsic stresses in amorphous thin films arise from systematic modifications of atomic positions after a slip-free adhesion layer forms with the substrate.[14] Such changes in atomic arrangement can be tailored by specific growth conditions. The PECVD input variables observed to exert the greatest influence on thin-film stress are deposition temperature,[13] hydrogen dilution,[15] plasma frequency,[16] discharge power,[17-19] and ambient gas pressure.[13] The influence of these deposition parameters on film structure consequently alters the mechanical and optoelectronic properties of the cells. In this study we isolate the influence of gas pressure.

The origin of stress in our films is likely due to an *ion bombardment effect*,[13,20,21] which has been previously reported in films deposited by both ion sputtering[20,22] and PECVD,[13,18] relating internal stresses of films to the momentum of the depositing ions. Based on models put forth by Windischmann[22] and Smets,[23] we are able to describe the observed stress behavior purely through ion interactions with the depositing film and correlate these descriptive models to the observed experimental data.

Intrinsic stress in amorphous silicon thin films can be viewed as a balance between two distinct but competing forces: the collapse of hydrogenated nanovoids after being formed on the depositing layer creating tensile stress,[24,25] and lattice expansion effects, which are responsible for the creation of compressive stresses in the film through the implantation of ions into the previously deposited layers[26] (often referred to as "ion

peening"). While plasma ion momentum dictates both of these forces, it is their relative strength at any given momentum level that determines the net intrinsic stress state of the film. Specifically, at low average ion momentum levels (for example, at high deposition pressure), the contribution of nanovoid collapse (either through interaction with the non-depositing ion plasma while still near the surface, or through ion injection collapsing more deeply buried voids) easily outweighs the compressive effects of bulk expansion from the relatively rare deep ion implantations, and thereby produces a film of net tensile stress. Conversely, with high ion momentum (low pressure), a substantially larger number of ions are implanted into the bulk of the film, resulting in a strong compressive stress component, outweighing the tensile stress from the collapse of nanovoids (especially as the voids available for collapse are inherently finite, whereas the limit to compressive stress from implantation does not contain such an abrupt limitation), and creating a net compressively stressed film. From these descriptions we conclude that our process conditions are determining the ion momentum of deposition, controlling both the collapse of nanovoids, and ion peening in our films, the balance of which is in turn dictating our film structure and intrinsic stress.

We justify the exclusive examination of ion bombardment-induced stresses through the elimination of all other plausible causes of stress in the material: given the growth parameters used in the present study, we exclude *surface stresses*[27] and *coalescence stresses,*[6,15] which dominate at film thicknesses of single nanometers. *Hydrogen and hydrogen-induced bond reconstruction*[28] models are precluded due to the observation of a strong tensile stress regime, as well as the lack of causal analysis present in these theories (see **Sec. III-C**). Nanocomposite effects[15] can also be reasonably concluded to play a negligible role as the growth temperature and hydrogen dilution ratios are too low to induce a partial phase transition to microcrystalline silicon.[29] Furthermore, we observe no evidence of embedded nanocrystals in the amorphous Si matrix via grazing-incidence X-ray diffraction. Finally, film compositional variations could be observed though changes in the deposition gas due to *silane dissociation*. However, results from Gallagher[30] indicate that for similar process conditions, deposition is dominated (>98%) by SiH_3 radicals, indicating that modifications to pressure and power could thus influence deposition rate (which is observed) but should not affect the chemical formulation of the depositing gas. This nearly constant deposition gas stoichiometry thus allows us to reasonably conclude that dissociation does not play a major role in the modification of structural properties in our study, although should likely be examined in those significantly varying deposition power or discharge frequency.

The remainder of this section is devoted to the elucidation of the ion bombardment model through the exploration of microstructural film properties, and the amalgamation of empirical and theoretical correlations. We will proceed in three steps: first, we will establish a numerical calculation of ion momentum (the property responsible for the control of ion bombardment) from our deposition conditions. Next, we will present a modified theoretical model of the compressive stress forces from the literature. Finally, we empirically include the tensile stress influences into our model by fitting the experimentally measured reduction in hydrogen void concentration.

B. Modeling Ion Bombardment through PECVD Conditions

To begin the numerical exploration of qualitative model described in the previous subsection, we calculate the average incident ion momentum through its relation to the average ion energy in the equation

$$\bar{p}_{\text{ion}} = \sqrt{2M\bar{E}_{\text{ion}}}\,, \qquad [3]$$

where M is the ion mass and $\bar{p}_{\text{ion}}$ is the average ion momentum. Through a reformulation of the theory proposed by Lee *et al.*,[17] average ion energy flux, $\bar{E}_{\text{ion}}$, can determined to vary as

$$\bar{E}_{\text{ion}} = \frac{qI_{\text{rms}}\lambda\cos\beta}{\omega\varepsilon_0 \text{A}_\text{p}}, \qquad [4]$$

where q is the electron charge, I_{rms} is the room mean square of the plasma current, λ is the mean free path of ions in the plasma, $\cos\beta$ the collision angle between the electric field and direction of ion propagation in the plasma (assumed 0.5, per Ref. 17), ω frequency (equal to $2\pi f$, where f is the nominal plasma frequency), ε_0 vacuum permittivity, and A_p is the electrode area. Here, ω and A_p are constant for all depositions. Translating I_{rms} into discharge power, W, and pressure in the deposition chamber, P, per Ref. 31, we obtain

$$\bar{p}_{\text{ion}} = \sqrt{2M\frac{q\lambda\sqrt{WP}\cos\beta}{\omega\varepsilon_0 \text{A}_\text{p}}}\,. \qquad [5]$$

Combining these variables with q and ε_0 into a constant term C, we are left with an expression for ion momentum as a function of our controllable deposition parameters and the ion mass and ion mean free path,

$$\bar{p}_{\text{ion}} = C\sqrt{M\lambda\sqrt{\frac{WP}{\omega}}}\,. \qquad [6]$$

The ion mean free path (λ) is inversely proportional to both the gas density and pressure present at deposition. Combining this relation with **Eq. 6**, results in our final formula for the ion momentum,

$$\bar{p}_{\text{ion}} \propto \left(\frac{W}{\omega P}\right)^{1/4}, \qquad [7]$$

showing a (-1/4) power dependence of process pressure on ion momentum, and allowing the relative determination of $\bar{p}_{\text{ion}}$ through our deposition conditions.

C. Implantation Effects on Stress

The direct relationship between compressive (bulk-implantation process) stress and ion momentum in sputtered films has been modeled theoretically by Davis,[26] yielding a proportionality of

$$\sigma \propto \frac{Y}{(1-\nu)} \frac{\bar{p}_{\text{ion}}}{R/j + k\bar{E}_{\text{ion}}^{5/3}}, \qquad [8]$$

where σ is the film stress, Y the Young's modulus, ν the Poisson ratio, $\bar{E}_{\text{ion}}$ is the deposition ion energy, $\bar{p}_{\text{ion}}$ is the average ion momentum, R/j is the ratio of deposition film flux to ion bombarding flux, and k is a constant material parameter. Following the analysis from Yi,[21] our PECVD deposition conditions will yield large R/j values (the majority of collisions with the film will be normal depositing collisions not bombardment collisions, in contrast to sputtering where the bombardment component can easily dominate that of deposition), and furthermore, due to our lack of argon dilution, the number of bombardment collisions should be at least roughly proportional to the total collisions. This, in agreement with calculations by Yi,[21] causes the stress to scale simply as

$$\sigma \propto \frac{Y}{(1-\nu)} \bar{p}_{\text{ion}}. \qquad [9]$$

It is important to note that this stress-momentum model applies to only the bulk (compressive) stress effects due to particle bombardment in fully densified films, free from microstructure modification, and thus with constant mechanical properties (Y and ν). To generalize this model further, we examine the dependence of the mechanical properties of the films on the evolving density.

Film Young's modulus in amorphous silicon has been modeled by Miranda *et al.*[32] to vary with a 2.5 power dependence on film density. The Poisson's ratio has been shown by Wehrspohn *et al.*[13] to remain virtually invariant across films of varying hydrogen content, and, through our examination, across all possible values (0 – ~0.3) imparts little change on the values obtained by **Eq. 9**. Combining these theories with **Eq. 9**, we are left with the equation

$$\sigma \propto \rho^{2.5} \bar{p}_{\text{ion}}. \qquad [10]$$

We validate our model by utilizing our experimental trend between density and ion momentum (fit simply to a second-order polynomial function, which, although not fit perfectly, does allow for the general influence of ion momentum on density to be incorporated) shown in **Fig. 3,** to fit **Eq. 10** to only one experimental variable ($\bar{p}_{\text{ion}}$). This final model of compressive stress is shown fit to our independently measured experimental stress data as the dashed line in **Fig. 4a**, matching a similar trend observed

in Ref. 33. One can note that the correlation between the model and experiment clearly breaks down in region **I** of the plot. This, however, can be accounted for through the inclusion of void collapse (tensile stress) effects (see **Sec. III-D**).

As a final note, while we exclude the hydrogen bonding model (see **Sec. III-A**) as an explanation of the total stress state in our films, we do not preclude the possibility of bombarded hydrogen influencing the stress state – as the aforementioned model (to our knowledge) makes no claims of the origin of the varying hydrogen content in the films, the theories could in fact be complementary: implantation of SiH_X radicals (as suggested in Ref. 23) would account for the correlation between compressive stress and hydrogen content observed in Ref. 27, and our analysis/model does not depend on the specific injected species (Si, H, or, most likely, a combination of the two) actually causing the induction of stress.

D. Void Collapse Effects on Stress

Through investigating the interplay between the effect of ion momentum (**Eq. 7**), on film porosity/density and film stress, we are able to clarify the underlying mechanisms responsible for tensile stress creation in our films.

Per **Sec. II-D**, the area under the ~2090 cm^{-1} infrared absorption peak is proportional to the concentration of hydrogen present in voids throughout the film, providing a numerical indication of hydrogen void concentration. **Fig. 4b** (in agreement with results observed by Hamers,[33,34] Smets,[23] and Wank[35] indicates that increasing ion momentum results in an initially rapid decrease in film porosity in the tensile region, followed by a nearly invariant low porosity in the compressive region.

We propose the modeling of tensile stress creation as proportional to the reduction of film porosity through the subtraction of the observed film hydrogen void concentration from an arbitrary baseline (representing the inherently created void concentration – see below). Combined with the trend of compressive stress arising from bulk effects (**Eq. 10**) we can produce the net stress influence displayed as the solid line in **Fig. 4a**, capturing the rounding of the stress-ion momentum curve (as seen in region **I** in **Fig. 4a**), as well as the previously fit compressive regime (region **II** in **Fig. 4a**). We dedicate the remainder of this subsection to justifying the two remaining assumptions of this model: first, that the two stress forces (compressive and tensile) apply across all deposition conditions, and second, that surface void formation is constant across our deposition conditions, with the observed reduction in hydrogen void concentration due purely to void collapse, and thus proportional to the tensile stress created.

Three aspects of our data support the conclusion that there are two independent stress forces applying across the entire range of our deposition conditions: first, the transition from tensile to compressive stress dominating in the films (shown as the beginning of region **II** in **Fig. 4**) occurs well before hydrogen void concentration has reached its minimum in the films. This shows that the concentration of voids is

continuing to be reduced in films well into the compressive stress regime, indicating that the tensile stress component is still present in the compressive regime, but merely being outweighed by the stronger implantation influences. Second, our model of compressive stress remains accurate far into the tensile regime, only beginning to deviate in region **I**, leveling off at the same location where film porosity begins to plateau as well, implying that even in the tensile stress regime, compressive stress is still playing a role in the net film stress state as well. Finally, we observe that silicon monohydride content (**Fig. 4b**) increases continuously with ion momentum, suggesting that bulk particle implantation of hydrogenated Si (the mechanism supposed to be responsible for the silicon monohydride in the material[23]) is occurring uniformly throughout our deposition range, and providing further evidence that bulk ion bombardment is indeed occurring throughout all deposition conditions, and lending credence to the theory that void collapse occurs from bulk bombardment even at low ion momentum levels. From this information we conclude that stress creation does indeed appear to be a balance between two separate phenomena responsible for tensile and compressive forces: In region **I**, the hydrogen void concentration is high, indicating that the level of void collapse is low, and thus the tensile stress is relatively low as well, responsible for the decrease in stress from the pure implantation model (dashed line) observed here. In the transition to region **II**, void concentration decreases, indicating that tensile stress is increasing. Compressive stress is increasing as well, however, initially driving the net stress to zero as the implantation influence takes over and finally, in region **II**, into a state of net compressive stress.

In our model of tensile stress creation we assert that the creation of porous nanovoids from the films surface evolution is fairly constant across our deposition conditions, which we justify here though the exclusion of the plausible mechanisms for altering the surface deposition geometry: while we are exploring the influence of ion bombardment on stress and structural properties, we are modifying this parameter through control of the deposition chamber pressure, which could possibly result in unintentional effects on the depositing surface geometry via changes to the plasma and depositing species stoichiometry, and through deviations in the deposition rate. As indicated by Doyle[36] and Gallager,[30] however, both the plasma composition and the depositing species across our process conditions should remain quite constant, which invalidates any influence that changes silane decomposition could have on the deposition surface (see **Sec. III-A**). Furthermore, while we do indeed observe fairly significant changes in the film rate of deposition, McCaughey[37] and Jalali-Jafari[24] have both demonstrated through molecular dynamics simulations that decreasing film deposition rate is shown to have either no effect, or to actually increase the inherent void creation, and conclude (as we assert here) that it is ion impact effects causing the observed decline in void concentration with increasing deposition rate (which we capture in the isolated compressive stress component model). Finally, we have measured surface roughness by atomic force microscopy (AFM), which shows no correlation to deposition conditions, further assuring us that the surface evolution is not being substantially altered by changes to the process pressure. From these factors, and the quality of the fit of the net stress (solid line in **Figs. 1** and **4a**) we conclude that tensile stress can be adequately modeled as proportional to the decrease in the film hydrogen void concentration from a constant level.

E. Failure of Stressed a-Si Films

Stable films were grown with intrinsic stresses ranging from -1253 to +387 MPa. Outside this stress range, one observes film buckling (compressive failure mode, **Fig. 2a**) and delamination (tensile failure mode, **Fig. 2b**). Extrapolation of the stress within failed films from their operating conditions predicts buckling and delamination film failure at approximately -1200 MPa and +450 MPa, respectively.

Two trends in our data are consistent with conclusions of other studies that applied mechanical stress to a-Si films at room temperature: (1) failure under tension occurs at lower absolute stress levels than under compression,[38-42] and (2) the absolute magnitude of compressive stress possible without failure is on the order of 1 GPa.[39,40,42]

VI. Conclusions

The results of this study provide an enhanced understanding of the origins of stress within a-Si:H thin films. We develop a semi-empirical model relating deposition conditions to stress creation and demonstrate further evidence of the microstructural forces contributing to stress in amorphous silicon. We show that compressive stress varies nearly linearly with depositing ion momentum, that tensile stress is controlled by hydrogen void destruction, and that the total intrinsic stress results from the balance between these two influences.

From these results, in combination with recent electrical transport[43,44] and optical measurements[35] reported elsewhere, a more complete picture of a-Si:H film process-structure-property relations begins to emerge. With the ability to predict film microstructure structure using empirical models, controllable a-Si:H properties should be achievable on a wide range of deposition systems.

V. Acknowledgements

Several people contributed to this work. E.J., S.C.-G., N.T., and T.B. conceived of the basic ideas for this work. E.J., S.C.-G., A.A., N.T., and M.I.B. designed and/or carried out experiments and interpreted the results. J. Elman (Filmetrics) and L. Shaw (MIT) provided Filmetrics support, and S. Speakman (MIT) provided X-ray diffraction support. E.J., S.C.-G., and N.T. fabricated samples. J.C.G., S.S., and T.B. supervised the research. E.J. and T.B. wrote the manuscript with extensive feedback from all co-authors. We acknowledge and thank C. Simmons (MIT), F. Spaepen (Harvard), E.A. Schiff (Syracuse University), and H. Branz (NREL) for helpful discussions. Funding was provided by the MIT-KFUPM Center for Clean Water and Energy. This work was performed in part at the Center for Nanoscale Systems (CNS), a member of the National

Nanotechnology Infrastructure Network (NNIN), which is supported by the National Science Foundation under NSF award no. ECS-0335765.

References

[1] G. D. Cody, B. Abeles, C. Wronski, C. R. Stephens, and B. Brooks, Solar Cells **2,** 227 (1980).

[2] F. Palma, in *Technology and applications of amorphous silicon*, edited by R. A. Streets (Springer-Verlag, Berlin Heidelberg, 2000), p. 309.

[3] M. A. Green, K. Emery, Y. Hishikawa, and W. Warta, Progress in Photovoltaics: Research and Applications **18,** 144 (2010).

[4] M. A. Green, *Silicon Solar Cells: Advanced Principles & Practice* (University of New South Wales, Sydney, Australia, 1995).

[5] T. Surek, in *3rd World Conference on Photovoltaic Energy Conversion*, *Vol. 3* (Osaka, Japan, 2003), p. 2507.

[6] L. B. Freund and S. Suresh, *Thin Film Materials: Stress, Defect Formation, and Surface Evolution* (Cambridge University Press, 2003).

[7] Z. Remes, M. Vanecek, P. Torres, U. Kroll, A. H. Mahan, and R. S. Crandall, Journal of Non-Crystalline Solids **227–230,** 876 (1998).

[8] A. A. Langford, M. L. Fleet, B. P. Nelson, W. A. Lanford, and N. Maley, Physical Review B **45,** 13367 (1992).

[9] A.H. Mahan, L.M. Gedvilas, J.D. Webb, Journal of Applied Physics **87**, 1650 (2000).

[10] H. Shanks, C. J. Fang, L. Ley, M. Cardona, F. J. Demond, and S. Kalbitzer, Physica Status Solidi b **100,** 43 (1980).

[11] A. H. M. Smets, W. M. M. Kessels, and M. C. M. v. d. Sanden, Applied Physics Letters **82,** 1547 (2003).

[12] P. J. Zanzucchi, C. R. Wronski, and D. E. Carlson, Journal of Applied Physics **48,** 5227 (1977).

[13] R. B. Wehrspohn, S. C. Deane, I. D. French, I. Gale, J. Hewett, M. J. Powell, and J. Robertson, Journal of Applied Physics **87,** 144 (2000).

[14] M. Ohring, *Materials Science of Thin Films*, 2nd ed. (Academic Press, 2002).

[15] Y. Q. Fu, J. K. Luo, S. B. Milne, A. J. Flewitt, and W. I. Milne, Materials Science and Engineering B **124-125,** 132 (2005).

[16] J. Dutta, U. Kroll, P. Chabloz, A. Shah, A. A. Howling, J.-L. Dorier, and C. Hollenstein, Journal of Applied Physics **72,** 3220 (1992).

[17] J. H. Lee, D. S. Kim, Y. H. Lee, and B. Farouk, Journal of the Electrochemical Society **143,** 1451 (1996).

[18] A. D. Glew, R. Saha, J. S. Kim, and M. A. Cappelli, Surface and Coatings Technology **114,** 224 (1999).

[19] V. Kulikovsky, V. Vorlíček, P. Boháč, M. Stranyánek, R. Čtvrtlík, and A. Kurdyumov, Thin Solid Films **516,** 5368 (2008).

[20] H. Windischmann, Journal of Applied Physics **62,** 1800 (1987).

[21] J. W. Yi, Y. H. Lee, B. Farouk, Thin Film Solids **326**, 154 (1998).

[22] H. Windischmann, Journal of Vacuum Science & Technology A **9,** 2431 (1991).

[23] A. H. M. Smets, W. M. M. Kessels, and M. C. M. vand de Sanden, Journal of Applied Physics **102**, 073523 (2007).

[24] B. Jalali-Jafari, H. Savaloni, and M. Gholipour-Shahraki, Physica Status Solidi (B) **244**, 3620 (2007).

[25] K.-H. Müller, Journal of Applied Physics **62**, 1796 (1987).

[26] C.A. Davis, Thin Film Solids **226**, 30 (1993).
[27] R. C. Cammarata., Progress in Surface Science **46,** 1 (1994).
[28] Y. Hishikawa, Journal of Applied Physics **62,** 3150 (1987).
[29] A. Matsuda, Journal of Non-Crystalline Solids **59–60,** 767 (1983).
[30] A. Gallagher, Journal of Applied Physics **63,** 2406 (1988).
[31] Y. Catherine and P. Couderc, Thin Solid Films **144,** 265 (1986).
[32] C.R. Miranda, K.V. Tretiakov, S. Scandolo, Journal of Non-Crystalline Solids **352**, 4283 (2006).
[33] E. A. G. Hamers, Acta Physica Slovaca **50**, 533 (2000).
[34] E. A. G. Hamers, W. G. J. H. M. van Sark, J. Bezemer, H. Meiling, and W.F. van der Weg, Journal of Non-Crystalline Solids **226**, 205 (1998).
[35] M. A. Wank, R. A. C. M. M. van Swaaij, P. Kudlacek, M. C. M. van de Sanden, and M. Zeman, Journal of Applied Physics **108**, 103304 (2010).
[36] J. R. Doyle, D. A. Doughty, and A. Gallagher, Journal of Applied Physics **68**, 4375 (1990).
[37] M. J. McCaughey, and M. J. Kushner, Journal of Applied Physics **65**, 186 (1989).
[38] H. Gleskova, I.-C. Cheng, S. Wagner, J. C. Sturm, and Z. Suo, Solar Energy **80,** 687 (2006).
[39] H. Gleskova, P. I. Hsu, Z. Xi, J. C. Sturm, Z. Suo, and S. Wagner, Journal of Non-Crystalline Solids **338–340,** 732 (2004).
[40] J. Gaspar, O. Paul, V. Chu, and J. P. Conde, J. Micromech. Microeng. **20,** 035022 (2010).
[41] H. Gleskova, S. Wagner, and Z. Suo, Applied Physics Letters **75,** 3011 (1999).
[42] T. N. Ng, W. S. Wong, R. A. Lujan, and R. A. Street, Advanced Materials **21,** 1855 (2009).
[43] M. A. Wank, R. van Swaaij, R. van de Sanden, and M. Zeman, Progress in Photovoltaics: Research and Applications. doi: 10.1002/pip.1157.
[44] G. Ganguly, I. Sakata, A. Matsuda, Journal of Non-Crystalline Solids **198-200**, 300 (1996).

Fig. 1

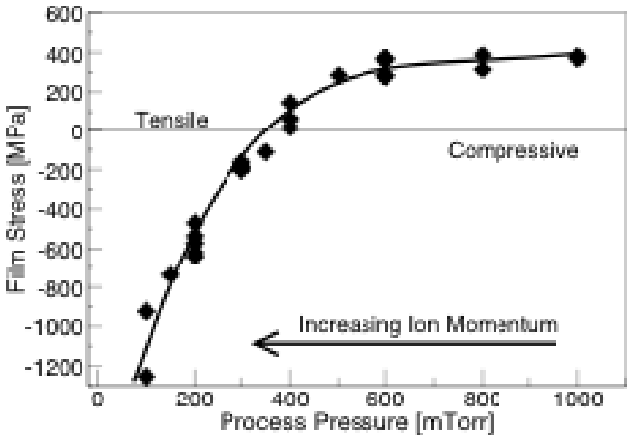

Fig. 1. Correlation between SiH_4 process pressure and measured film stress. The solid line displays the correlation with the net stress model, as described in **Sec. III-D**, and the thin line through the origin simply denotes the transition between net tensile and compressive stress.

Fig. 2

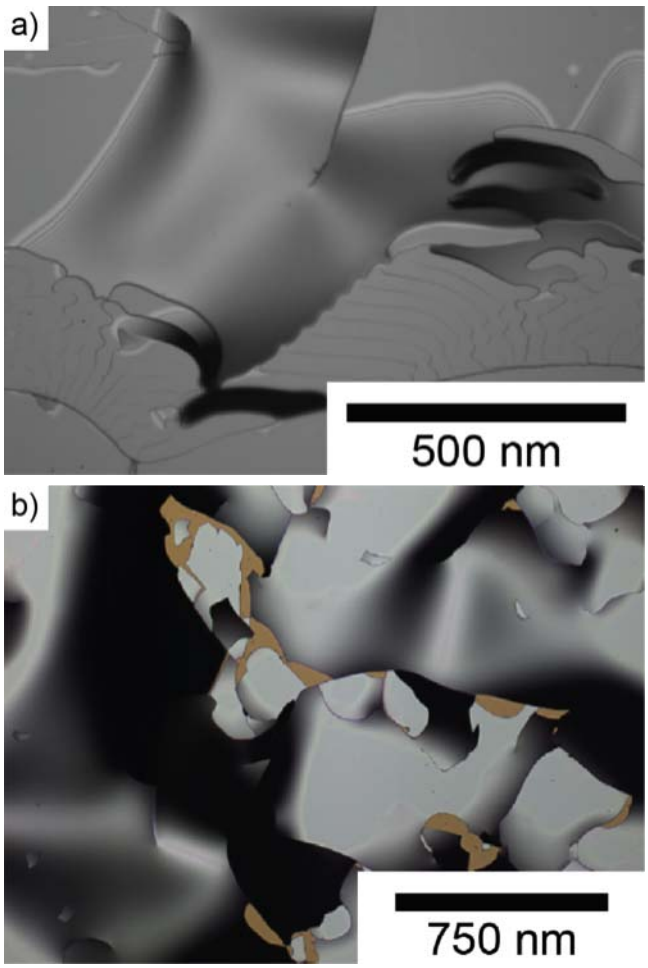

Fig. 2. Optical micrographs of films exhibiting failure from (a) compressive stress buckling, estimated -1200 MPa and (b) tensile stress delamination, estimated +450 MPa.

Fig. 3

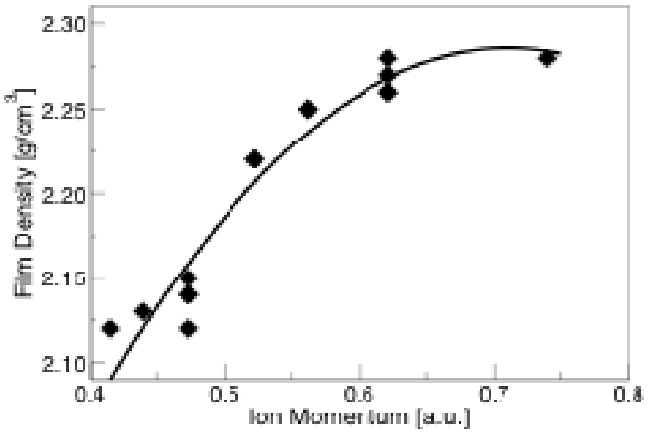

Fig. 3. Film density (determined optically) with respect to deposition ion momentum, shown with the second-order polynomial fit used for the inclusion of the evolving mechanical properties of films in **Eq. 10**.

Fig. 4

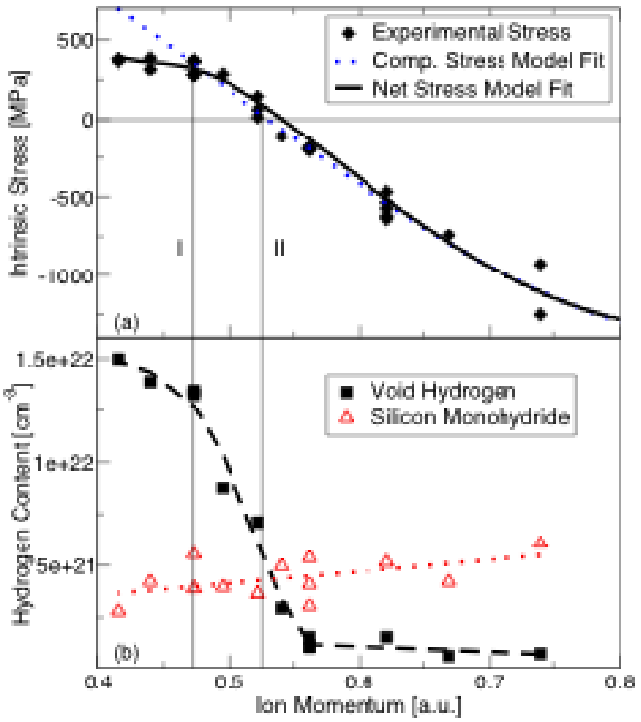

Fig. 4 (a): Film intrinsic stress as a function of ion momentum $\bar{p}_{\text{ion}}$, defined in **Eq. 7**, shown with the fits to compressive stress (**Eq. 10**) and net (compressive + tensile) stress. **(b)**: Hydrogen content and distribution in IR bonding configurations correlated to deposition ion momentum, with regressions shown as guides to the eye. Regions **I** and **II** are described in the text.